Perspective

Prussian Blue Analogs as Battery Materials

Kevin Hurlbutt,[1,†] Samuel Wheeler,[1,†] Isaac Capone,[1] Mauro Pasta[1,*]

[1] Department of Materials, University of Oxford, Parks Road, Oxford OX1 3PH, United Kingdom
[†] These authors contributed equally to the work.
* Correspondence: mauro.pasta@materials.ox.ac.uk

Context & Scale

In this work, we offer our perspective on a class of compounds known as Prussian blue analogs, a group of versatile cyano-coordination polymers. Originally commercialized in the dye industry, they have more recently been used in diverse energy technologies including energy storage, electrocatalysts, and thermal power generation. We address their role as components of the next-generation of batteries with improved cycle life and power capability. Through a review of achievements from early electrochemical experiments to crystallographic breakthroughs to development of state-of-the-art electrodes, we outline how control over the crystal structure allows these materials' electrochemistry to be finely tuned for diverse use cases. Despite recent advances, there remain conspicuous and fundamental questions about the structure-electrochemistry relationship that we identify. We adumbrate investigations using density functional theory calculations, synchrotron X-ray techniques, electrochemical tests, and technoeconomic analysis to answer those questions.

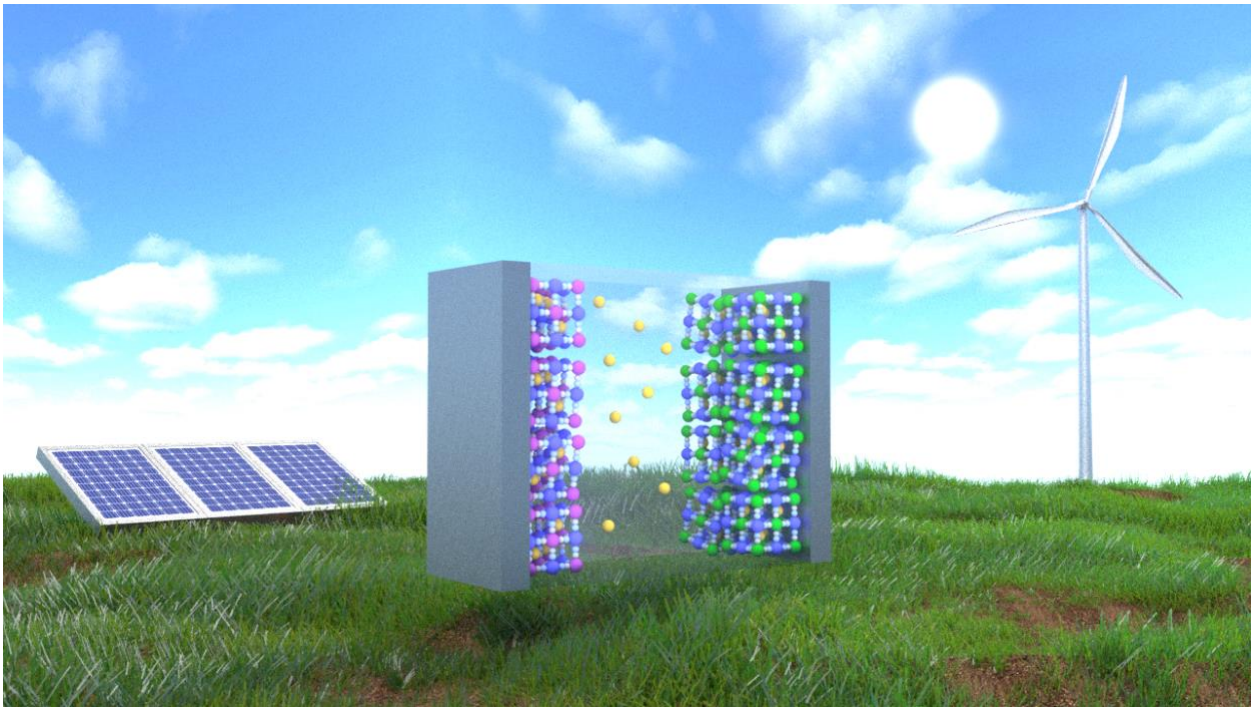

Figure 1. Prussian Blue Analog Batteries Enabling Renewable but Intermittent Energy Sources.

Summary

Prussian blue analogs have significant promise as active materials for the next generation of battery electrodes with improved cycle life and rate capability. Their useful electrochemical properties include two independent redox centers per unit cell; a nanoporous, open framework for rapid ion conduction; high stability during ion (de)insertion; and structural and electrochemical tunability for diverse applications. Here we share insights into how control of the five main crystallographic features (two transition-metal ions, the inserting ion, defects, and water) imparts control over the ion-insertion reaction. **We then identify five key opportunities to expand our understanding of these materials**, including the role of water in their ion conduction, modelling, synthesis methods, use as anode materials, and technoeconomics. Further research in these areas will accelerate the development of new, high-performing battery electrodes.

Introduction

Prussian blue analogs (PBAs) are a class of materials that have garnered substantial, renewed interest recently because of their unique properties, several of which are highly desirable in energy storage. First, they have a high specific capacity for inserting alkali and alkali earth metals via a reversible, two-electron reaction.[1] Second, their cubic geometry and the wide channels of their nanoporous, open-framework structure ensure rapid ionic conduction for high rate capability.[2] Third, they experience minimal change to their geometry during ion insertion, which imparts impressively long cycle lives.[3] Fourth, these compounds are prepared via a simple and inexpensive co-precipitation reaction between aqueous precursors.[4] Finally, their properties are highly tunable and adaptable for different applications.[5,6] The primary disadvantage to PBAs is their low crystal density (1.96 g cm^{-3} for defect-free sodium iron hexacyanoferrate), which is less than half that of high-performing lithium-ion cathodes.[7,8] Because of these unique strengths and limitations, PBAs have primarily been applied in stationary, grid-scale energy storage where energy-density requirements are more lax, but where cost, cycle life, and rate capability are key (**Figure 1**).

These intriguing electrochemical properties arise from the interaction of the crystal structure with inserting ions. The general electrochemical equation for the insertion of an alkali metal into a PBA is given by:

$$A_xP^J[R^K(CN)_6]_{1-y} \cdot wH_2O + A^+ + e^- \rightarrow A_{x+1}P^J[R^{K-1}(CN)_6]_{1-y} \cdot wH_2O$$

in which A is an alkali metal ion, and P and R are transition metal ions octahedrally coordinated to six cyanide ligands via the nitrogen and carbon atom, respectively (**Figure 2**).[9] The value *y* is the fraction of vacancies of the hexacyanoferrate complex ion (the primary lattice defect). Water, both zeolitic and coordinated to deficiently bonded metal ions at vacancies, can also be present.

While several review articles have recently been published on PBA electrode materials,[10–12] here we offer our perspective on the often-subtle relationship between these five tunable crystallographic features and the ion-insertion reaction, exploring the effect that each of these has on the insertion. From there we examine **five underexplored areas in PBA research**: water in ion conduction, modelling, synthesis methods, use as anode materials, and technoeconomics. It is our aim to introduce what has already been achieved in the design of PBA battery components and to highlight those research areas most important to accelerating the development of future PBA-based energy storage.

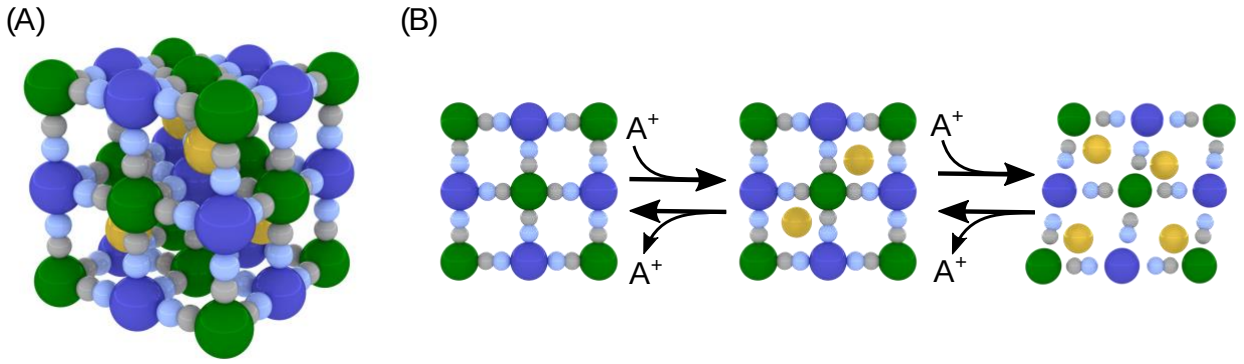

Figure 2. The Crystal Structure of PBAs. (A) PBAs have a face-centered cubic geometry and open-framework lattice. Here the green and dark blue atoms are transition-metal ions at the R site and P site, respectively. The yellow atoms are inserting ions. Gray atoms are carbon and light blue are nitrogen. (B) Alkali metal ions insert into the sub-cubes of the lattice as the transition-metal ions change oxidation state. At high concentrations of lithium or sodium, the structure can distort to a less symmetric rhombohedral geometry.

Effect of Lattice Architecture on Electrochemistry

The element at the (carbon-coordinated) **R site** sits at the center of the hexacyanometallate complex from which PBAs get their open framework and cubic geometry (*fm3m* space group).[13] The R–C bond length strongly affects the lattice parameter and channel size, which in turn determine the ionic conductivity. Substitution with an element of smaller atomic radius decreases the lattice parameter.[14] Counterintuitively, chemical reduction also decreases the lattice parameter, despite the insertion of an ion into the sub-cube. This is because the added electron density causes the hexacyanometallate complex to contract. For example, the volume of the unit cell in manganese hexacyanoferrate decreases 3.5% on lithiation,[15] and other compositions have shown similar volume changes on insertion of different alkali ions.[16] This high degree of reversibility leads to extremely long cycles lives. As the R site is the typical center for redox activity in a PBA, the chosen element determines the reaction potential. The hexacyanochromate(III/II) and hexacyanomanganate(III/II) redox pairs have reaction potentials around -0.8 and 0 V versus the standard hydrogen electrode (SHE), respectively.[5] However, the great majority of research into PBA batteries has focused on the hexacyanoferrates as positive electrodes because of their high reaction potential of 1 V versus SHE and ease of synthesis. This is well within the stability window of water (about -0.18 to 1.05 V versus SHE at pH 3), so they have often been cycled in aqueous electrolyte. The Fe–C bond in the hexacyanoferrates is stable up to at least 200 °C[17] and within the pH range 2 to 6 with solubility increasing with pH as cyanide undergoes ligand exchange with hydroxide groups.[18] This stability makes PBAs attractive as safe battery materials despite the presence of cyanide ligands.

Compared to the R site, the **P site** has enjoyed a much richer variety of substitution in the pursuit of practical PBA electrodes. The geometry does not change under substitution at the P site (with the notable exception of zinc[19]). The lattice parameter, and thus the channel size, depends linearly on the ionic radius of the P-site cation.[20] The reaction potential at the R site is affected by the P-site ion, with higher ionic potentials (the quotient of charge and radius) leading to a higher insertion potential. This is due to greater polarization of the σ bond in the cyanide ligand, more significant π backbonding, and lower energy of the t_{2g} orbitals on the R-site ion.[5] Zinc, copper, and nickel are three common choices for the P site that are usually inactive electrochemically. The hexacyanoferrate compounds of these metals have achieved relatively low specific capacities of around 60 mA h g^{-1} at potentials within the electrochemical stability window of water. Cui and coworkers developed these materials for stationary storage with excellent rate capability and cycle life.[21,22] Iron, manganese, and cobalt, in contrast, are electrochemically active within the stability window of organic electrolytes, allowing for two-electron redox reactions. This allows for the

full utilization of the crystal structure for ion storage. Accessing this total capacity for the two-electron reaction (170 mA h g^{-1} in the case of defect-free sodium iron hexacyanoferrate[23]) results in two voltage plateaus.[24] These cathodes have lower cycle lives because structural water reacts at these elevated potentials[6] and because of changes to the crystal structure as the P-site ion changes oxidation state. Manganese in its +3 oxidation state is susceptible to a Jahn-Teller distortion,[25] while the ionic radius of cobalt decreases from 0.745 to 0.545 Å as it undergoes a spin-state transition from its high-spin +2 state to the low-spin +3 state on oxidation.[26] The deleterious effect of geometric changes on long-term cyclability is an important factor in PBA design. Finally, an exciting research direction today is the preparation of single-phase, solid-solution PBAs with two elements at the P site. Properties like lattice parameter and reaction potential of these solutions are averages of the corresponding properties of the pure materials. The lattice parameter in a solid-solution (manganese, cobalt) hexacyanoferrate has been shown to be simply the average of the lattice parameters of the two pure compounds, weighted by mass fraction.[27] Similarly, the voltage and capacity of a PBA can be tuned in a (copper, nickel) hexacyanoferrate by controlling composition.[28] This mixing strategy has the potential to ameliorate the disadvantages of the most promising materials, by, for instance, preventing phase transitions on cycling.

Positive electrodes have been prepared for inserting ions from the alkali, alkali earth, and transition metals including lithium,[29] sodium,[6] potassium,[30] rubidium,[31] cesium,[32] calcium,[33] magnesium,[34] aluminum,[35] and zinc.[36] Lithium, sodium, and potassium are the most commonly investigated inserting ions, and they occupy the **A site** at the center of the lattice's sub-cube (**Figure 3A**). Thermodynamically, the inserting ion determines the free energy of the insertion reaction. The insertion potential for the monovalent ions follows the order $K^+ > Na^+ > Li^+$ in copper hexacyanoferrate (0.93, 0.8, and ~0.7 V versus SHE)[37] and, similarly, $Cs^+ > Rb^+ > K^+ > Na^+ > Li^+$ in nickel hexacyanoferrate (1.3, 0.9, 0.7, 0.6, and 0.4 V versus SHE)[31] in aqueous electrolyte. This correlation between increasing ionic radius and increasing reaction potential holds for multivalent ions as well.[38] This is due to the large contribution of the hydration energy (which is a function of the ionic potential) to the Gibbs free energy of ion insertion.[5] Density functional theory (DFT) calculations further theorize that larger inserting ions have stronger steric interactions, leading to higher potentials.[39] They also suggest that larger inserting ions preferentially sit within vacancies rather than the center of the sub-cubes. Indeed, experiments confirm that cesium and rubidium, among other large ions, occupy defect sites.[38,40] The smallest ions also have a lower-energy position off the center of the sub-cubes. Lithium and sodium displace toward the corners in the <111> direction.[41] Above a critical concentration, the lattice cooperatively displaces in the <111> direction as well, resulting in a rhombohedral geometry (**Figure 3B**). This structural change can decrease ionic conductivity and reversibility, lowering rate capability and cycle life, respectively. The benefits of high capacity in lithium- and sodium-ion electrodes must be weighed against sacrifices to these other performance metrics. Kinetically, the ease of movement of ions via the nanoporous <100> channels (**Figure 3C**) is determined by the ratio of the ionic radius to the lattice parameter. The diffusion coefficient for lithium has been observed to increase from $4.6 \cdot 10^{-10}$ to $3.5 \cdot 10^{-9}$ cm^2 s^{-1} as the lattice parameter increases from 10.56 to 10.70 Å. Sodium's diffusion coefficient is smaller, but also increases with lattice parameter from $2.3 \cdot 10^{-10}$ to $7.7 \cdot 10^{-10}$ cm^2 s^{-1}.[42] The R-, P-, and A-site ions must be chosen so that the channel size provides adequate ionic conductivity for whatever (dis)charge rate requirements are specified for the application. Broader interest in sodium-ion batteries generally has resulted in substantial work on sodium-ion PBA cathodes in the last few years. Lithium insertion has received less attention recently because of its low potential, severe <111> displacement, and the general superiority of existing lithium-ion cathodes. PBAs remain, however, one of the only active materials capable of inserting potassium, and we expect even more work on potassium-ion PBA batteries in the near future. Inserting

ions like rubidium are more expensive and lack any viable anode materials. High-energy metal anodes require an organic electrolyte, and are particularly interesting for di- and trivalent metals. However, they require a hydration shell to shield their local charge within the PBA cathode lattice.[43] Zinc, as a water-stable metal anode, is an exception and has garnered recent interest as the A-site species in a PBA battery.[44,45]

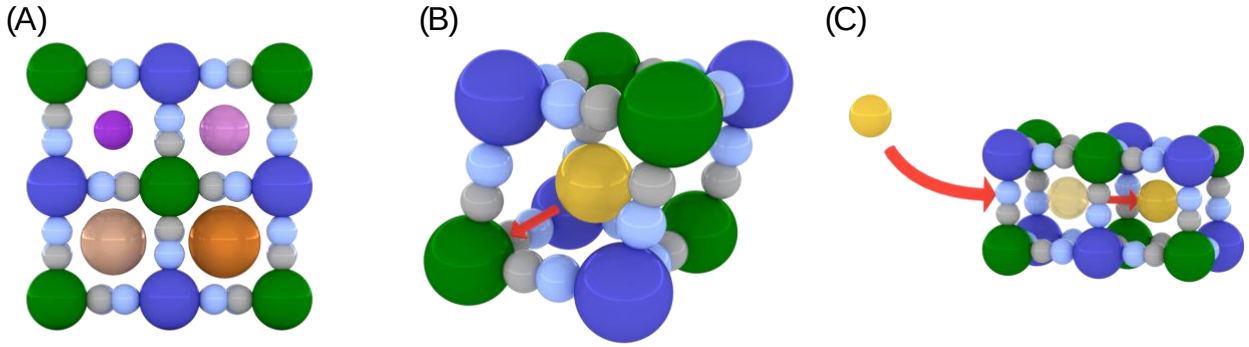

Figure 3. Metal Ions Inserting into the PBA Structure. (A) The PBA lattice can accommodate diverse metal ions at the A site. Here the relative sizes of (clockwise from top left) lithium, sodium, rubidium, and potassium are shown. (B) High concentrations of lithium and sodium ions can induce a cubic-to-rhombohedral phase change in PBAs as the inserting ion displaces toward the corner of the sub-cube. (C) The inserting ions diffuse through the structure via the <100> channels.

Vacancies of the hexacyanometallate complex are the primary structural defect in PBAs (**Figure 4A**). They have two beneficial impacts on electrode performance. First, vacancy-mediated transport through the bulk increases ionic conductivity.[40] Connected cavities offer an alternative route to inserting ions other than the <100> channels, and there is evidence to suggest that vacancies are the primary or exclusive means of conduction for larger ions (**Figure 4B**). Second, vacancies have a stabilizing effect on the crystal structure. The Jahn-Teller distortion only occurs below a minimum vacancy content.[46] It is possible that vacancies also contribute to minimizing the <111> cooperative displacement that can occur at higher levels of lithiation and sodiation. These two benefits result in improved rate capability and cycle life. However, the obvious disadvantage to high vacancy content is that, as a positively charged defect, it reduces the specific capacity. Increasing energy density therefore requires methods of synthesis that minimize vacancies. A common synthetic strategy for vacancy reduction is the use of excess alkali ion during synthesis; one study determined that an increase in sodium nitrate from 1 to 5 M decreased vacancy from 19% to 7% and increased sodium ions per formula unit from 1.24 to 1.72.[47] More sophisticated methods include the use of a single transition-metal source[23,48] and chelating agents such as citrate.[49,50] Yang and coworkers have used the citrate-assisted synthesis to achieve vacancies as low as 1% in a cobalt hexacyanoferrate for sodium-ion, with a reversible specific capacity of 150 mA h g^{-1}, which is approaching the theoretical maximum.[51] They also reported improved cycle life compared to the high-vacancy material, which they attributed to higher electronic conductivity. In general, though, new and improved methods of vacancy suppression will also need to be judged for their scalability. One of the virtues of PBAs is their easy synthesis, and each added synthetic step makes manufacturing more complicated and expensive.

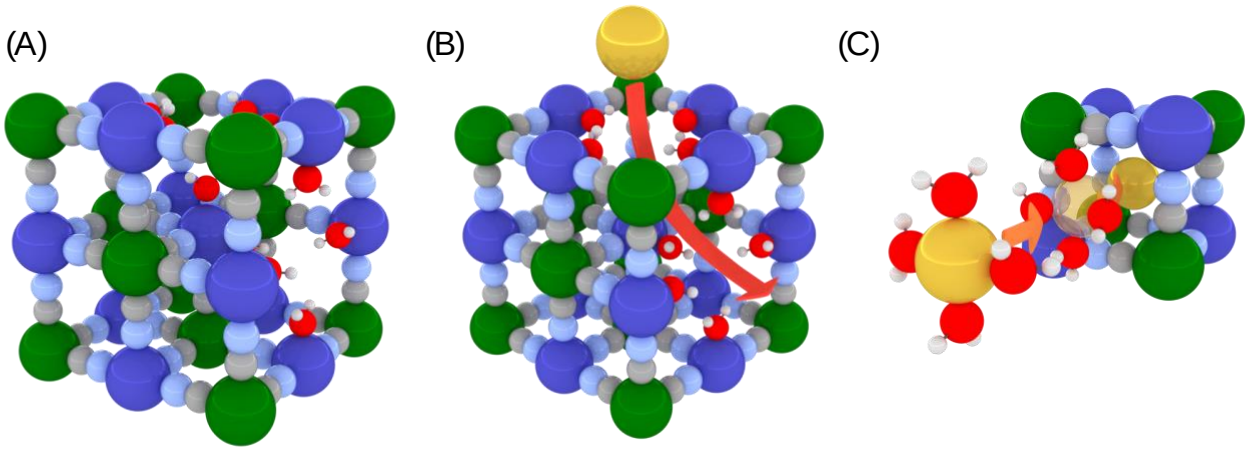

Figure 4. Defects and Water Affecting the Ion Insertion Reaction. (A) Two vacancies of the hexacyanometallate complex, including the R-site ion and its six cyanide ligands, are shown: one on the top face and one on the right-front face. (B) Connected vacancies offer an alternate route for the conduction of ions through the structure. (C) An inserting ion sheds its hydration shell before entering the lattice.

Experiments with neutron and X-ray diffraction on both single-crystal and powder PBAs have identified two structurally distinct positions for **water molecules**.[52,53] The first type is zeolitic water, which occupies the A site in competition with the inserting ion. The second type of water coordinates to the exposed P-site ions at vacancies. These water molecules' electronegative oxygen atoms help shield the large positive charge of the exposed transition-metal ions. The correlation between vacancies and water is positive because each additional vacancy exposes an additional P-site ion for coordination and also increases the volume available for zeolitic water. Zeolitic water is removed more easily than coordinated water as it is bonded more weakly.[54] Water can influence the thermodynamically favored phase; it solvates lithium and sodium, decreasing their effective ionic potential and mitigating the cubic-to-rhombohedral shift. And for high-voltage reactions in organic electrolyte, the active material must be aggressively dried because any excess water will cause side reactions and lower coulombic efficiency. Goodenough and coworkers have used a vacuum drying procedure to prepare iron hexacyanoferrate[48] and manganese hexacyanoferrate,[54] each of which achieved a capacity of about 150 mA h g^{-1}, which is comparable to Yang's cobalt hexacyanoferrate and is approaching theoretical. Goodenough carried out XRD studies on the manganese PBA and determined that it had distorted to a rhombohedral geometry when heavily sodiated. It is possible that the complete removal of all water makes more severe the structural distortions that accompany high concentrations of small inserting ions. Doping the P site with electrochemically inactive metals like nickel is an active area of research to maintain the structurally stabilizing benefits of vacancies and water without the negative effects on capacity and coulombic efficiency.[55]

Critical Research Fronts

Having addressed the state-of-the-art in the design of PBAs for battery cathodes, we turn our attention to those areas of research in which we see critical gaps in knowledge. Driving forward work in the following areas will allow higher-performing PBA materials to be developed faster for new battery applications.

The role of water in ionic conduction is complicated and poorly understood. A paddlewheel mechanism has been proposed for ion movement through channels and vacancies.[37] In this model, coordinated water rotates around its bond access with a P-site ion at a vacancy which can help move inserting ions. However, it has also been found that the removal of some zeolitic water dramatically increases conductivity.[56] Besides the bulk conductivity, the interfacial charge transfer kinetics are far more favorable in aqueous

electrolyte compared to organic, because in aqueous electrolyte the inserting ion only needs to shed its solvent sphere partially as it moves from the outer Helmholtz zone to the inner Helmholtz zone (**Figure 4C**).[57] The higher activation energy arising from further desolvation leads to a higher overpotential and slower kinetics. One study has found the activation energy for sodium insertion increases from 5.1 kJ mol^{-1} in aqueous electrolyte to 51.0 kJ mol^{-1} in organic.[58] Goodenough has established some important computational insights into energetic effects of water's presence.[59] Further theory and targeted experiments, like nuclear magnetic resonance spectroscopy or isotopic labeling studies, can differentiate the roles of zeolitic and coordinated water in ion conduction.

There is a general lack of fundamental understanding about the nucleation and growth mechanism of PBAs in solution. PBAs are typically synthesized through a simple and inexpensive co-precipitation reaction. An aqueous solution of the hexacyanometallate compound is combined with an aqueous solution of a salt (often a halide) of the transition metal that will occupy the P site. The final coordination polymer forms immediately. The ease of synthesis makes PBAs highly scalable as battery materials. Furthermore, parameters like salt concentration, temperature, and mixing rate can be controlled to impart some control over defects and water content. Generally, though, the co-precipitation methods results in high vacancy and water content. Recently more advanced methods have been developed to suppress vacancies,[60] and increasingly elaborate, functional architectures, like core-shell particles made of two separate phases, are being realized. The growth of PBA crystals can be observed from nuclei via *in situ* small-angle X-ray scattering (SAXS), and microfluidic reactors can allow for precise control over mixing rates and salt concentrations to study their effect on vacancies. A more detailed description of the reaction mechanism will increase the tunability of lattice architecture and electrochemistry.

A quantitative description of the PBA electronic structure is key to understanding important properties like electronic conductivity, but only very limited work on computational models of PBAs has been done so far. There is substantial opportunity for a robust model of PBAs within DFT to understand and suggest methods of improving electronic conductivity. Furthermore, computational models can accelerate the process of discovering new useful compositions. Wojdeł and coworkers undertook the pioneering DFT work in PBAs in the mid 2000s.[61,62] Eventually they were able to calculate several properties for a limited number of compositions using the generalized gradient approximation (GGA+U) method. This strategy was taken up by Mizuno and coworkers to model the effect of the inserting ion's radius on insertion[39] and by Lopez and coworkers to calculate additional properties for the iron hexacyanoferrate system.[63] The calculation of the band structure for hypothetical compounds can reveal information about important materials properties. However, the critical, semi-empirical Hubbard parameter is known for only a few compositions. A database of Hubbard parameters, an efficient means of calculating them, or rapid experimental techniques for their determination would enable predictive DFT models of PBAs. Such models can select the most promising candidates for time-intensive synthesis and characterization.

The behavior of PBAs is poorly characterized at low potentials. The need for a negative electrode that matches the rate capability and high cycle life of the positive electrodes has motivated work into PBA anodes with different R-site ions. Manganese hexacyanomanganate has been investigated and utilized as an anode in combination with a PBA cathode. The resulting full cell delivered a voltage of 1.55 V and retained 90% capacity at 12 C because the two electrodes were well matched in terms of kinetics and stability.[64] Attempts have been made to develop other compositions that operate at even lower potentials and in an organic electrolyte, but success remains elusive. The hexacyanoferrates[65] and hexacyanocobaltates[66] have been explored as anodes for lithium-ion, but they do not maintain their crystal structure at such low potentials. At present, the limits of the stability of water in the structure and the structure itself are unknown. Better understanding of their behavior at low potential will aid in

designing future compositions. Given the need for low-potential materials and the extraordinary number of unsynthesized and uncharacterized PBAs, we see the development of low potential PBA materials as an important research direction in the future. A possible group of candidate are the hexacyanochromates, which show electrochemical activity at low potentials in aqueous electrolytes.[5]

Finally, **no thorough cost analysis of PBA batteries has been published that** can direct research toward practical applications. We therefore created a concise technoeconomic model that broadly identifies which use-cases are addressable by PBA batteries (**Figure 5**). The performance and cost of three PBA battery chemistries were modeled using capacity, voltage, and density data from state-of-the-art components. Values for many of the parameters were taken from the BatPaC modelling software.[67]

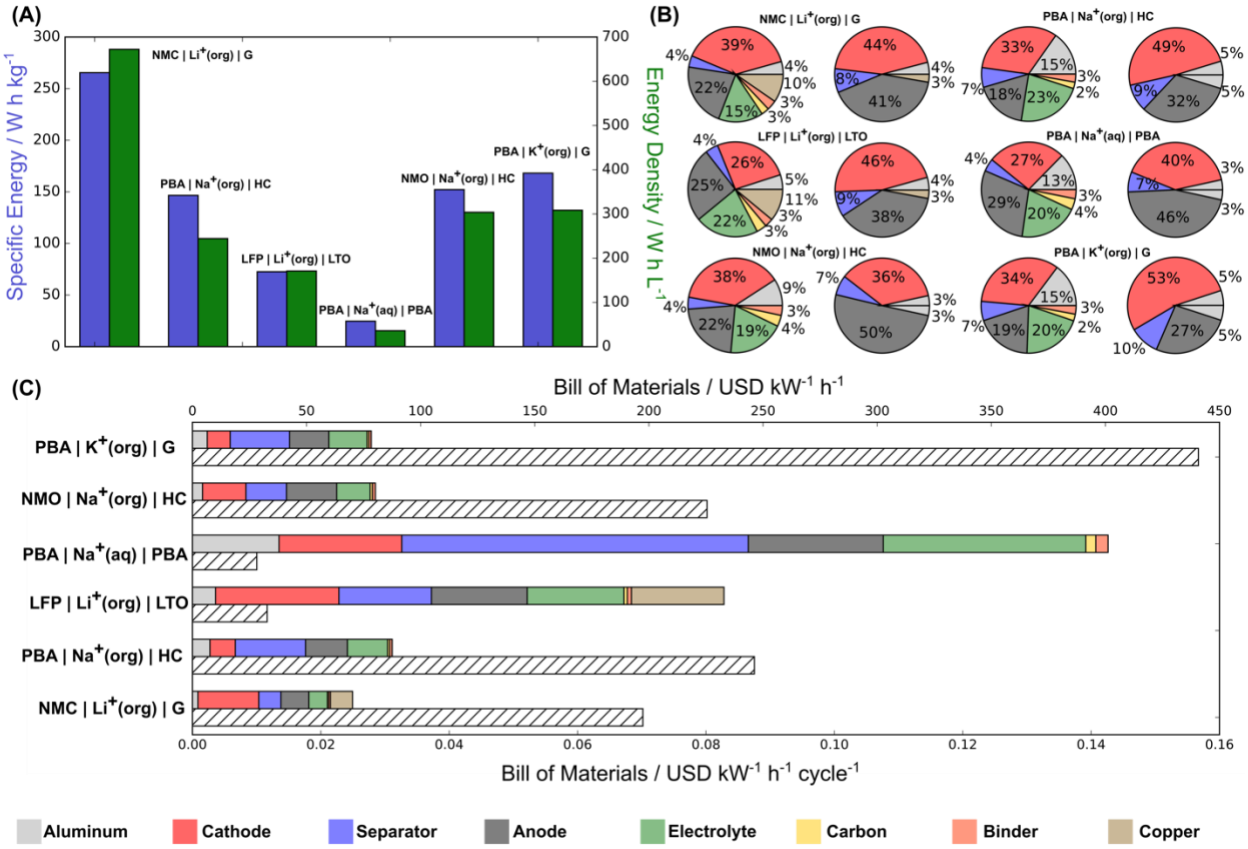

Figure 5. A Concise Technoeconomic Model of PBA Batteries. Three different PBA batteries were modeled, as well as three other systems for the purposes of comparison. The modeled chemistries are: lithium nickel-manganese-cobalt oxide 622 (NMC) | Li^+ in organic electrolyte (org) | graphite (G); sodium PBA | Na^+(org) | hard carbon (HC); lithium iron phosphate (LFP) | Li^+(org) | lithium titanate (LTO); sodium manganese oxide (NMO) | Na^+(org) | HC; sodium PBA | Na^+(aq) | sodium PBA; and potassium PBA | K^+(org) | G. The values for many parameters were taken from the BatPaC modelling package, and the NMO is based on that modeled by Passerini in a recent perspective[68]. The model extends only to the stack level; each system has a cathode of about 80 µm thickness. (A) The specific energy (blue bars, left axis) and energy density (green bars, right axis) are plotted for the three PBA architectures analyzed, as well as two lithium-ion stacks and one sodium-ion stack for context. (B) The mass fraction (left) and volume fraction (right) are plotted for the components of the six architectures. The slices in the charts are color-coded according to the legend at the bottom. The two lithium-ion stacks also contain copper current collectors because lithium alloys with aluminum at low potentials. (C) The bill of materials in USD kW^{-1} h^{-1} (colored bars, upper axis) are plotted. The bar segments are also color-coded according to the legend at bottom. The cost amortized over cycle life is also shown (hashed bars, lower axis).

As **Figure 5A** shows, the specific energy and energy density of all PBA batteries are substantially lower than those of state-of-the-art lithium-ion batteries. The energy density is especially low because of their very low crystal density. For this reason, PBA batteries are unlikely candidates for use in consumer electronics or electric vehicles. Comparing the mass-fractions of the components of the sodium-ion PBA and sodium-ion NMO batteries, shown in **Figure 5B**, the PBA cathode is significantly less massive (33% vs. 38%) but thicker (49% vs. 36%). The bill of materials for each architecture has also been calculated based on estimates on the prices of the stack components. **Figure 5C** shows the bill, broken up by component and normalized by energy content. PBAs have a low cost because they are easily and scalably prepared from inexpensive precursors.[4] Our model uses a value of 5.00 USD kg^{-1} for PBAs. The potassium-ion PBA battery is cost-competitive with the sodium-ion NMO battery modeled by Passerini.[68] The sodium-ion PBA | PBA battery has a very high cost at about 400 USD kW^{-1} h^{-1}. But when its bill of materials is amortized over its extremely long cycle life, the cost falls below even the lithium-ion LFP | LTO system (a common technology in stationary energy storage). This metric, price in units of USD kW^{-1} h^{-1} $cycle^{-1}$, is a more relevant metric for stationary storage like utility deployments.[69] Furthermore, the impressive rate capability of PBA batteries allows them to respond quickly to changes in load without significant loss of capacity or damage to the PBA crystal structure. For these reasons, commercial deployments of PBA batteries to date have been in grid-scale applications. Indeed, the U.S. Department of Energy has supported the development and scale-up of PBA batteries through two multi-million dollar grants to Natron Energy[70] (formerly Alveo Energy) and Sharp.[71] The caveat is, of course, that the all PBA battery will have a much higher up-front capital cost for an (e.g.) 1 MW h energy-storage installation. In summary, while the low crystal density of PBAs will prevent their near-term application in fields like consumer electronics or electric vehicles, their inexpensive precursors, long cycle lives, and high rate capabilities make them technoeconomically competitive with contemporary grid-scale energy-storage technology. More sophisticated modelling can extend the analysis to the cell or pack level using BatPaC, treat the power capabilities in a quantitative manner, or examine exact PBA compositions with more specific cost and performance parameters.

Conclusion

Here we have outlined our perspective on the intricate relationship between the crystal structure and electrochemistry of PBAs at each crystallographic component: both the carbon- and nitrogen-coordinated transition-metal ions, the inserting ion, vacancies, and water. Careful control at each of these sites has led to the current array of state-of-the-art PBA compositions in batteries. We also described gaps in the current understanding of these materials. Specifically, the role of water in conduction is poorly understood and will strongly impact organic-electrolyte cells. Fundamental understanding of the PBA polymerization reaction is necessary to optimize synthesis conditions. Better computational tools will help improve electronic conductivity and speed materials discovery. Most low-potential PBAs that could serve as anodes have not been synthesized or explored. And low energy density, long cycle life, low cost applications with sodium, potassium, or other metal ion charge carriers are ideal for PBA electrodes. Deeper fundamental understanding and further technological development are likely to make PBAs an important active material in the future portfolio of electrochemical energy storage solutions.

Acknowledgements

The authors gratefully acknowledge the contributions of their collaborators and coworkers mentioned in the cited references. This publication arises from research funded by the John Fell Oxford University Press Research Fund. M.P. is indebted to EPSRC for financial support.

Acknowledgements

The authors declare no competing interests.

References

1. Itaya, K., Uchida, I., and Neff, V.D. (1986). Electrochemistry of polynuclear transition metal cyanides: Prussian blue and its analogues. Acc. Chem. Res. *19*, 162–168.
2. Moritomo, Y., Takachi, M., Kurihara, Y., and Matsuda, T. (2012). Thin Film Electrodes of Prussian Blue Analogues with Rapid Li^+ Intercalation. Appl. Phys. Express *5*, 041801.
3. Matsuda, T., and Moritomo, Y. (2012). Two-Electron Reaction without Structural Phase Transition in Nanoporous Cathode Material. J. Nanotechnol. *2012*, 1–8.
4. Bauer, A., Song, J., Vail, S., Pan, W., Barker, J., and Lu, Y. (2018). The Scale-up and Commercialization of Nonaqueous Na-Ion Battery Technologies. Adv. Energy Mater. *8*, 1702869.
5. Scholz, F., and Dostal, A. (1996). The Formal Potentials of Solid Metal Hexacyanometalates. Angew. Chemie Int. Ed. *34*, 2685–2687.
6. Lu, Y., Wang, L., Cheng, J., and Goodenough, J.B. (2012). Prussian Blue: a new framework of electrode materials for sodium batteries. Chem. Commun. *48*, 6544–6546.
7. Buser, H.J., Ludi, A., Schwarzenbach, D., and Petter, W. (1977). The Crystal Structure of Prussian Blue: $Fe_4[Fe(CN)_6]_3 \cdot xH_2O$. Inorg. Chem. *16*, 2704–2710.
8. Chiang, Y.-M., Jang, Y.-I., Wang, H., Huang, B., Sadoway, D.R., and and Ye, P. (1998). Synthesis of $LiCoO_2$ by Decomposition and Intercalation of Hydroxides. J. Electrochem. Soc. *145*, 887.
9. Keggin, J.F., and Miles, F.D. (1936). Structures and formulae of the Prussian blues and related compounds. Nature *137*, 577–578.
10. Qian, J., Wu, C., Cao, Y., Ma, Z., Huang, Y., Ai, X., and Yang, H. (2018). Prussian Blue Cathode Materials for Sodium-Ion Batteries and Other Ion Batteries. Adv. Energy Mater. *1702619*, 1–24.
11. Xu, Y., Zheng, S., Tang, H., Guo, X., Xue, H., and Pang, H. (2017). Prussian blue and its derivatives as electrode materials for electrochemical energy storage. Energy Storage Mater. *9*, 11-30
12. Wang, B., Han, Y., Wang, X., Bahlawane, N., Pan, H., Yan, M., Jiang, Y., Wang, H., Wang, Y., Yan, N., *et al.* (2018). Prussian blue analogues for rechargeable batteries. ISCIENCE. Available at 10.1016/j.isci.2018.04.008.
13. Dostal, A., Kauschka, G., Reddy, S.J.J., and Scholz, F. (1996). Lattice contractions and expansions accompanying the electrochemical conversions of Prussian blue and the reversible and irreversible insertion of rubidium and thallium ions. J. Electroanal. Chem. *406*, 155–163.
14. Ludi, A., and Güdel, H. (1973). Structural chemistry of polynuclear transition metal cyanides. Inorg. Chem. *14*, 1–21.
15. Okubo, M., Asakura, D., Mizuno, Y., Kim, J.-D.D., Mizokawa, T., Kudo, T., and Honma, I. (2010). Switching Redox-Active Sites by Valence Tautomerism in Prussian Blue Analogues $A_xMn_y[Fe(CN)_6] \cdot nH_2O$ (A: K, Rb): Robust Frameworks for Reversible Li Storage. J. Phys. Chem. Lett. *1*, 2063–2071.
16. Wessells, C.D., Huggins, R.A., and Cui, Y. (2011). Copper hexacyanoferrate battery electrodes with long cycle life and high power. Nat. Commun. *2*, 550.
17. Peng, J., Wang, J., Yi, H., Hu, W., Yu, Y., Yin, J., Shen, Y., Liu, Y., Luo, J., Xu, Y., *et al.* (2018). A Dual-Insertion Type Sodium-Ion Full Cell Based on High-Quality Ternary-Metal Prussian Blue Analogs. Adv. Energy Mater. *8*, 1702856.
18. Yang, Y., Brownell, C., Sadrieh, N., May, J., Del Grosso, A., Place, D., Leutzinger, E., Duffy, E., He, R., Houn, F., *et al.* (2007). Quantitative measurement of cyanide released from Prussian Blue. Clin. Toxicol. *45*, 776–781.
19. Rodríguez-Hernández, J., Reguera, E., Lima, E., Balmaseda, J., Martínez-García, R., and Yee-Madeira, H. (2007). An atypical coordination in hexacyanometallates: Structure and properties of hexagonal zinc phases. J. Phys. Chem. Solids *68*, 1630–1642.

20. Matsuda, T., Kim, J., Ohoyama, K., and Moritomo, Y. (2009). Universal thermal response of the Prussian blue lattice. Phys. Rev. B *79*, 172302.
21. Wessells, C.D., Peddada, S. V, Huggins, R.A., and Cui, Y. (2011). Nickel hexacyanoferrate nanoparticle electrodes for aqueous sodium and potassium ion batteries. Nano Lett. *11*, 5421–5425.
22. Pasta, M., Wessells, C.D., Huggins, R.A., and Cui, Y. (2012). A high-rate and long cycle life aqueous electrolyte battery for grid-scale energy storage. Nat. Commun. *3*, 1149.
23. Guo, Y.-G.Y., You, Y., Wu, X.X.-L., and Yin, Y.Y.-X. (2014). High-quality prussian blue crystals as superior cathode materials for room-temperature sodium-ion batteries. Energy Environ. Sci. *7*, 1643-1647
24. Bie, X., Kubota, K., Hosaka, T., Chihara, K., and Komaba, S. (2018). Synthesis and electrochemical properties of Na-rich Prussian blue analogues containing Mn, Fe, Co, and Fe for Na-ion batteries. J. Power Sources *378*, 322–330.
25. Moritomo, Y., Wakaume, K., Takachi, M., Zhu, X., and Kamioka, H. (2013). Li^+ intercalation of manganese ferrocyanide as investigated by in situ valence-differential absorption spectroscopy. J. Phys. Soc. Japan *82*, 1–6.
26. Takachi, M., Matsuda, T., and Moritomo, Y. (2013). Cobalt Hexacyanoferrate as Cathode Material for Na^+ Secondary Battery. Appl. Phys. Express *6*, 025802.
27. Pasta, M., Wang, R.Y., Ruffo, R., Qiao, R., Lee, H.-W., Shyam, B., Guo, M., Wang, Y., Wray, L.A., Yang, W., *et al.* (2016). Manganese–cobalt hexacyanoferrate cathodes for sodium-ion batteries. J. Mater. Chem. A *4*, 4211–4223.
28. Wessells, C.D., McDowell, M.T., Peddada, S.V., Pasta, M., Huggins, R.A., and Cui, Y. (2012). Tunable reaction potentials in open framework nanoparticle battery electrodes for grid-scale energy storage. ACS Nano *6*, 1688-1694
29. Imanishi, N., Morikawa, T., Kondo, J., Takeda, Y., Yamamoto, O., Kinugasa, N., and Yamagishi, T. (1999). Lithium intercalation behavior into iron cyanide complex as positive electrode of lithium secondary battery. J. Power Sources *79*, 215–219.
30. Bie, X., Kubota, K., Hosaka, T., Chihara, K., and Komaba, S. (2017). A novel K-ion battery: hexacyanoferrate(II)/graphite cell. J. Mater. Chem. A *5*, 4325–4330.
31. Lee, H.-W., Pasta, M., Wang, R.Y., Ruffo, R., and Cui, Y. (2014). Effect of the Alkali Insertion Ion on the Electrochemical Properties of Nickel Hexacyanoferrate Electrodes. Faraday Discuss. *176*, 69–81.
32. Chen, R., Tanaka, H., Kawamoto, T., Asai, M., Fukushima, C., Na, H., Kurihara, M., Watanabe, M., Arisaka, M., and Nankawa, T. (2013). Selective removal of cesium ions from wastewater using copper hexacyanoferrate nanofilms in an electrochemical system. Electrochim. Acta *87*, 119–125.
33. Padigi, P., Goncher, G., Evans, D., and Solanki, R. (2015). Potassium barium hexacyanoferrate - a potential cathode material for rechargeable calcium ion batteries. J. Power Sources *273*, 460–464.
34. Wang, R.Y., Wessells, C.D., Huggins, R. a, and Cui, Y. (2013). Highly reversible open framework nanoscale electrodes for divalent ion batteries. Nano Lett. *13*, 5748–52.
35. Reed, L.D., Ortiz, S.N., Xiong, M., and Menke, E.J. (2015). A rechargeable aluminum-ion battery utilizing a copper hexacyanoferrate cathode in an organic electrolyte. Chem. Commun. *51*, 14397–14400.
36. Liu, Z., Pulletikurthi, G., and Endres, F. (2016). A Prussian Blue/Zinc Secondary Battery with a Bio-Ionic Liquid-Water Mixture as Electrolyte. ACS Appl. Mater. Interfaces *8*, 12158–12164.
37. Wessells, C.D., Peddada, S. V., McDowell, M.T., Huggins, R. a., and Cui, Y. (2012). The Effect of Insertion Species on Nanostructured Open Framework Hexacyanoferrate Battery Electrodes. J. Electrochem. Soc. *159*, A98.
38. Wang, R.Y., Shyam, B., Stone, K.H., Weker, J.N., Pasta, M., Lee, H.W., Toney, M.F., and Cui, Y.

(2015). Reversible Multivalent (Monovalent, Divalent, Trivalent) Ion Insertion in Open Framework Materials. Adv. Energy Mater. *5*, 1–10.

39. Ling, C., Chen, J., and Mizuno, F. (2013). First-principles Study of Alkali and Alkaline Earth Ion Intercalation in Iron Hexacyanoferrate: the Important Role of Ionic Radius. J. Phys. Chem. C. *117*, 21158-21165.
40. Moritomo, Y., Igarashi, K., Kim, J., and Tanaka, H. (2009). Size Dependent Cation Channel in Nanoporous Prussian Blue Lattice. Appl. Phys. Express *2*, 085001.
41. Moritomo, Y., Matsuda, T., Kurihara, Y., and Kim, J. (2011). Cubic-Rhombohedral Structural Phase Transition in $Na_{1.32}Mn[Fe(CN)_6]_{0.83}\cdot 3.6H_2O$. J. Phys. Soc. Japan *80*, 074608.
42. Takachi, M., Fukuzumi, Y., and Moritomo, Y. (2016). Na^+ diffusion kinetics in nanoporous metal-hexacyanoferrates. Dalt. Trans. *45*, 458–461.
43. Lipson, A.L., Pan, B., Lapidus, S.H., Liao, C., Vaughey, J.T., and Ingram, B.J. (2015). Rechargeable Ca-Ion Batteries: A New Energy Storage System. Chem. Mater. *27*, 8442–8447.
44. Zhang, L., Chen, L., Zhou, X., and Liu, Z. (2015). Morphology-Dependent Electrochemical Performance of Zinc Hexacyanoferrate Cathode for Zinc-Ion Battery. Sci. Rep. *5*, 1–11.
45. Trócoli, R., and La Mantia, F. (2014). An Aqueous Zinc-Ion Battery Based on Copper Hexacyanoferrate. ChemSusChem. *8*, 481-485.
46. Kurihara, Y., Matsuda, T., and Moritomo, Y. (2013). Structural Properties of Manganese Hexacyanoferrates against Li Concentration. Jpn. J. Appl. Phys. *52*, 017301.
47. Moritomo, Y., Kurihara, Y., Matsuda, T., and Kim, J. (2011). Structural Phase Diagram of Mn--Fe Cyanide against Cation Concentration. J. Phys. Soc. Jpn. *80*, 8–11.
48. Wang, L., Song, J., Qiao, R., Wray, L.A., Hossain, M. a., Chuang, Y.-D., Yang, W., Lu, Y., Evans, D., Lee, J.-J., *et al.* (2015). Rhombohedral Prussian White as Cathode for Rechargeable Sodium-Ion Batteries. J. Am. Chem. Soc. *137*, 2548-2554.
49. Chen, R., Huang, Y., Xie, M., Wang, Z., Ye, Y., Li, L., and Wu, F. (2016). Chemical inhibition method to synthesize highly crystalline prussian blue analogs for sodium-ion battery cathodes. ACS Appl. Mater. Interfaces *8*, 31669–31676.
50. Li, C., Zang, R., Li, P., Man, Z., Wang, S., Li, X., Wu, Y., Liu, S., and Wang, G. (2018). High Crystalline Prussian White Nanocubes as a Promising Cathode for Sodium-ion Batteries. Chem. - An Asian J. *13*, 342–349.
51. Wu, X., Wu, C., Wei, C., Hu, L., Qian, J., Cao, Y., Ai, X., Wang, J., and Yang, H. (2016). Highly Crystallized $Na_2CoFe(CN)_6$ with Suppressed Lattice Defects as Superior Cathode Material for Sodium-Ion Batteries. ACS Appl. Mater. Interfaces *8*, 5393–5399.
52. Beall, G.W., Milligan, W.O., Korp, J., and Bernal, I. (1977). Crystal structure of $Mn_3[Co(CN)_6]_2\cdot 12H_2O$ and $Cd_3[Co(CN)_6]_2\cdot 12H_2O$ by Neutron and X-Ray Diffraction. Inorg. Chem. *16*, 2715–2718.
53. Herren, F., Fischer, P., Ludi, A., Hälg, W., and Haelg, W. (1980). Neutron diffraction study of Prussian Blue, $Fe_4[Fe(CN)_6]_3.xH_2O$. Location of water molecules and long-range magnetic order. Inorg. Chem. *19*, 956–959.
54. Song, J., Wang, L., Lu, Y., Liu, J., Guo, B., Xiao, P., Lee, J.-J., Yang, X.-Q., Henkelman, G., and Goodenough, J.B. (2015). Removal of Interstitial H_2O in Hexacyanometallates for a Superior Cathode of a Sodium-Ion Battery. J. Am. Chem. Soc. *137*, 2658-2664.
55. Moritomo, Y., Urase, S., and Shibata, T. (2016). Enhanced battery performance in manganese hexacyanoferrate by partial substitution. Electrochim. Acta *210*, 963–969.
56. Perez-Cappe, E., Aguilar-Frutis, M., Chavez, N., Ribalta, J., and Reguera, E. (2012). Cation mobility in a series of zeolite-like coordination polymers. Microporous Mesoporous Mater. *163*, 326–333.
57. Mizuno, Y., Okubo, M., Asakura, D., Saito, T., Hosono, E., Saito, Y., Oh-ishi, K., Kudo, T., and Zhou, H. (2012). Impedance spectroscopic study on interfacial ion transfers in cyanide-bridged coordination polymer electrode with organic electrolyte. Electrochim. Acta *63*, 139–145.

58. Mizuno, Y., Okubo, M., Hosono, E., Kudo, T., Zhou, H., and Oh-ishi, K. (2013). Suppressed Activation Energy for Interfacial Charge Transfer of a Prussian Blue Analog Thin Film Electrode with Hydrated Ions (Li^+, Na^+ and Mg^{2+}). J. Phys. Chem. C *117*, 6–11.
59. Xiao, P., Song, J., Wang, L., Goodenough, J.B., and Henkelman, G. (2015). Theoretical study of the structural evolution of a $Na_2FeMn(CN)_6$ cathode upon Na intercalation. Chem. Mater. *27*, 3763–3768.
60. Zakaria, M.B., and Chikyow, T. (2017). Recent advances in Prussian blue and Prussian blue analogues: synthesis and thermal treatments. Coord. Chem. Rev. *352*, 328–345.
61. Wojdeł, J.C., and Bromley, S.T. (2004). Efficient calculation of the structural and electronic properties of mixed valence materials: Application to Prussian Blue analogues. Chem. Phys. Lett. *397*, 154–159.
62. Wojdeł, J.C., Moreira, I.D.P.R., and Illas, F. (2009). Periodic density functional theory study of spin crossover in the cesium iron hexacyanochromate prussian blue analog. J. Chem. Phys. *130*, 014702.
63. Hegner, F.S., Galán-Mascarós, J.R., and López, N. (2016). A Database of the Structural and Electronic Properties of Prussian Blue, Prussian White, and Berlin Green Compounds through Density Functional Theory. Inorg. Chem. *55*, 12851–12862.
64. Firouzi, A., Qiao, R., Motallebi, S., Valencia, C.W., Israel, H.S., Fujimoto, M., Wray, L.A., Chuang, Y.-D., Yang, W., and Wessells, C.D. (2018). Monovalent manganese based anodes and co-solvent electrolyte for stable low-cost high-rate sodium-ion batteries. Nat. Commun. *9*, 861.
65. Shibata, T., Takachi, M., and Moritomo, Y. (2017). Low Voltage Charge/Discharge Behavior of Manganese Hexacyanoferrate. Batteries *3*, 7.
66. Nie, P., Shen, L., Luo, H., Ding, B., Xu, G., Wang, J., and Zhang, X. (2014). Prussian blue analogues: a new class of anode materials for lithium ion batteries. J. Mater. Chem. A *2*, 5852–5857.
67. Nelson, P.A., Gallagher, K.G., Bloom, I., and Dees, D.W. (2011). Modeling the Performance and Cost of Lithium-Ion Batteries for Electric-Drive Vehicles. Argonne Natl. Lab., 1–102.
68. Vaalma, C., Buchholz, D., Weil, M., and Passerini, S. (2018). A cost and resource analysis of sodium-ion batteries. Nat. Rev. Mater. *3*, 18013.
69. Barnhart, C.J.C., and Benson, S.M.S. (2013). On the importance of reducing the energetic and material demands of electrical energy storage. Energy Environ. Sci. *6*, 1083.
70. Bomgardner, M.M. (2015). ARPA - E Shows Off Its Big Batteries. Chem. Eng. News *93*, 21–22.
71. LaMonica, M. (2012). Beyond Lithium Ion : ARPA-E Places Bets on Novel Energy Storage. MIT Technol. Rev.

Figures

Figure 1. Prussian Blue Analog Batteries Enabling Renewable but Intermittent Energy Sources.

Figure 2. The Crystal Structure of PBAs. (A) PBAs have a face-centered cubic geometry and open-framework lattice. Here the green and dark blue atoms are transition-metal ions at the R site and P site, respectively. The yellow atoms are inserting ions. Grey atoms are carbon and light blue are nitrogen. (B) Alkali metal ions insert into the sub-cubes of the lattice as the transition-metal ions change oxidation state. At high concentrations of lithium or sodium, the structure can distort to a less symmetric rhombohedral geometry.

Figure 3. Metal Ions Inserting into the PBA Structure. (A) The PBA lattice can accommodate diverse metal ions at the A site. Here the relative sizes of (clockwise from top left) lithium, sodium, rubidium, and potassium are shown. (B) High concentrations of lithium and sodium ions can induce a cubic-to-rhombohedral phase change in PBAs as the inserting ion displaces toward the corner of the sub-cube. (C) The inserting ions diffuse through the structure through the <100> channels.

Figure 4. Defects and Water Affecting the Ion Insertion Reaction. (A) Two vacancies of the hexacyanometallate complex, including the R-site ion and its six cyanide ligands, are shown: one on the top face and one on the right-front face. (B) Connected vacancies offer up an alternate route for the conduction of ions through the structure. (C) An inserting ion sheds its hydration shell before entering the lattice.

Figure 5. A Concise Technoeconomic Model of PBA Batteries. Three different PBA batteries were modeled, as well as three other systems for the purposes of comparison. The modeled chemistries are: lithium nickel-manganese-cobalt oxide 622 (NMC) | Li^+ in organic electrolyte (org) | graphite (G); sodium PBA | Na^+(org) | hard carbon (HC); lithium iron phosphate (LFP) | Li^+(org) | lithium titanate (LTO); sodium manganese oxide (NMO) | Na^+(org) | HC; sodium PBA | Na^+(aq) | sodium PBA; and potassium PBA | K^+(org) | G. The values for many parameters were taken from the BatPaC modelling package, and the NMO is based on that modeled by Passerini in a recent perspective[68]. The model extends only to the stack level; each system has a cathode of about 80 µm thickness. (A) The specific energy (blue bars, left axis) and energy density (green bars, right axis) are plotted for the three PBA architectures analyzed, as well as two lithium-ion stacks and one sodium-ion stack for context. (B) The mass fraction (left) and volume fraction (right) are plotted for the components of the six architectures. The slices in the charts are color-coded according to the legend at bottom. The two lithium-ion stacks also contain copper current collectors because lithium alloys with aluminum at low potentials. (C) The bill of materials in USD kW^{-1} h^{-1} (colored bars, upper axis) are plotted. The bar segments are also color-coded according to the legend at bottom. The cost amortized over cycle life is also shown (hashed bars, lower axis).